Pacific Decadal Variability: The Tropical Pacific Mode and the North Pacific Mode[*]

L. Wu, Z. Liu, and R. Gallimore

Center for Climatic Research, University of Wisconsin—Madison, Madison, Wisconsin

R. Jacob

Argonne National Laboratory, Argonne, Illinois

D. Lee and Y. Zhong

Center for Climatic Research, University of Wisconsin—Madison, Madison, Wisconsin

ABSTRACT

Pacific decadal variability is studied in a series of coupled global ocean–atmosphere simulations aided by two "modeling surgery" strategies: partial coupling (PC) and partial blocking (PB). The PC experiments retain full ocean–atmosphere coupling in selected regions, but constrain ocean–atmosphere coupling elsewhere by prescribing the model climatological SST to force the atmospheric component of the coupled system. In PB experiments, sponge walls are inserted into the ocean component of the coupled model at specified latitudinal bands to block the extratropical–tropical oceanic teleconnection.

Both modeling and observational studies suggest that Pacific decadal variability is composed of two distinct modes: a decadal to bidecadal tropical Pacific mode (TPM) and a multidecadal North Pacific mode (NPM). The PC and PB experiments showed that the tropical Pacific mode originates predominantly from local coupled ocean–atmosphere interaction within the tropical Pacific. Extratropical–tropical teleconnections, although not a necessary precondition for the genesis of the tropical decadal variability, can enhance SST variations in the Tropics. The decadal memory in the Tropics seems to be associated with tropical higher baroclinic modes. The North Pacific mode originates from local atmospheric stochastic processes and coupled ocean–atmosphere interaction. Atmospheric stochastic forcing can generate a weaker NPM-like pattern in both the atmosphere and ocean, but with no preferred timescales. In contrast, coupled ocean–atmosphere feedback can enhance the variability substantially and generate a basin-scale multidecadal mode in the North Pacific. The multidecadal memory in the midlatitudes seems to be associated with the delayed response of the subtropical/subpolar gyre to wind stress variation in the central North Pacific and the slow growing/decaying of SST anomalies that propagate eastward in the Kuroshio Extension region. Oceanic dynamics, particularly the advection of the mean temperature by anomalous meridional surface Ekman flow and western boundary currents, plays an important role in generating the North Pacific mode.

1. Introduction

Recent observational studies have identified distinct decadal–interdecadal climate variability in the midlatitude and tropical Pacific (e.g., Nitta and Yamada 1989; Trenberth and Hurrell 1994; Graham 1994; Deser and Blackmon 1995; Zhang et al. 1997; Mantua et al. 1997; Enfield and Mestas-Nunez 1999; Garreaud and Battisti 1999). The low-frequency variability has been linked to marine biological cycles and climate variation over North America (Latif and Barnett 1994, 1996; Mantua et al. 1997; Barlow et al. 2001). The causes and origins of the Pacific decadal variability, however, are not fully understood (Miller and Schneider 2000). One school of thought proposes that Pacific decadal variability is generated primarily within the North Pacific (Latif and Barnett 1994; Barnett et al. 1999a) and may teleconnect to the Tropics via the atmosphere (Barnett et al. 1999b; Pierce et al. 2000) and/or ocean (McCreary and Lu 1994; Liu et al. 1994; Lysne et al. 1997). Another school of thought suggests that low-frequency variability in the Pacific is generated over the entire extratropical–tropical climate system in conjunction with feedbacks associated with extratropical–tropical interactions in the ocean and atmosphere (Gu and Philander 1997; Kleeman et al. 1999). Other studies hypothesize that Pacific decadal

variability is intrinsically tropically driven (Tziperman et al. 1995; Yukimoto et al. 1996; Knutson and Manabe 1998; Schneider 2000) and may affect the midlatitudes through atmospheric teleconnection (Trenberth 1990; Graham 1994). Finally, low-frequency variability in the Pacific may also be a consequence of the reddening effect of atmospheric stochastic forcing by the ocean (Hasselmann 1976; Frankignoul et al. 1997; Jin 1997; Saravanan and Mc Williams 1997; Weng and Neelin 1998).

Recent observational studies suggest that Pacific decadal variability may consist of more than one variability mode, most notably, an ENSO-like bidecadal mode and a North Pacific multidecadal mode (Deser and Blackmon 1995; Zhang et al. 1997; Nakamura et al. 1997; Minobe 1997; Enfield and Mestas-Nunez 1999; Barlow et al. 2001). These studies indicate the possibility of multiple origins and mechanisms for decadal climate variability in the Pacific. However, the causes of the climate variability are difficult to identify directly from observations, because of the difficulty in separating out all the complex feedbacks.

In this study, we designed a set of experiments using a coupled ocean–atmosphere general circulation model [Fast Ocean–Atmosphere Model (FOAM), Jacob 1997] to identify the origins of Pacific decadal climate variability. Some preliminary results have been presented in Liu et al. (2002). Based on the results of these experiments, we propose that the ENSO-like bidecadal tropical Pacific mode (TPM) and multidecadal North Pacific mode (NPM) are generated largely internally within the tropical and North Pacific, respectively. In addition, tropical–extratropical teleconnections can also enhance tropical climate variability substantially.

To identify the origins of these decadal modes, two ''modeling surgery'' strategies are developed. The first approach, partial coupling (PC), constrains ocean–atmosphere coupling in some selected regions but prescribes simulated climatological SSTs to force the model atmosphere elsewhere. The second approach, partial blocking (PB), is used to block the extratropical–tropical oceanic exchange by inserting a sponge wall in a specific latitudinal band of the ocean component of the coupled system. The combination of PC and PB provides an important modeling surgical technique for assessing the role of coupled ocean–atmosphere feedbacks (with PC) and teleconnections within the ocean (with PB) in generating climate variability (Liu et al. 2002; Wu and Liu 2002).

The paper is organized as follows. A brief description of the model is provided in section 2. In section 3, evidence is given for decadal TPM and NPM in both observation and coupled model simulations. Section 4 describes in detail the PC and PB modeling surgery approaches. Sections 5 and 6 are devoted to the study of the origins of the North and tropical Pacific decadal variability, respectively. Concluding remarks and further discussion are provided in section 7.

2. The model (FOAM)

We used FOAM1.0 developed jointly at the University of Wisconsin—Madison and the Argonne National Laboratory (Jacob 1997). The atmospheric model is a fully parallel version of the National Center for Atmospheric Research (NCAR) Community Climate Model version 2 (CCM2) [Parallel Community Climate Model version 2 (PCCM2) at R15] but with the atmospheric physics replaced by those of CCM3. The ocean model is conceptually similar to the Geophysical Fluid Dynamics Laboratory (GFDL) Modular Ocean Model (MOM) with a resolution of 1.4° latitude × 2.8° longitude and 16 vertical levels, and is designed for massively parallel platforms. A simple thermodynamic sea ice model is incorporated. Without flux adjustment, the fully coupled model has been run for 850 yr showing no apparent climate drift. The last 400 yr of simulation is used for the analysis in this study.

To provide a reference for the basic model variability, we compare the model ENSO with the observed ENSO. The leading EOF of the anomalous model SST within the interannual band (<8 yr) captures the main features of the observed ENSO (see Fig. 1 of Liu et al. 2000); the area-weighted pattern correlation between the model and observed EOFs is 0.82. Overall, FOAM simulates a reasonable ENSO variability with a realistic timescale and an amplitude of about 75% of the observed ENSO (Liu et al. 2000).

3. Pacific decadal variability

a. Observational evidence of decadal SST variability

The main observational dataset used in this study is the reconstruction of historical SST anomalies generated by Kaplan et al. (1998, hereafter K98) on a 5° × 5° grid for the period 1856–1999. Since Pacific decadal variability involves the entire basin, unrotated EOFs may not be able to separate regional physical modes due to the orthogonal constraints on both the spatial and temporal EOF components. Here we apply a varimax rotation to the ordinary EOFs to extract variability modes. A detailed analysis of the unrotated EOF and rotated EOF (REOF) of Pacific decadal variability can be found in Barlow et al. (2001). To focus on interdecadal timescales, most analyses are performed after the data are low-pass filtered to retain variability longer than 8 yr.

Figure 1 shows the first and third REOF modes of the observed annual mean SST anomalies over the Pacific basin. These two modes explain 30% and 12% of the total decadal variance, respectively.[1] The first REOF

---

[1] The second REOF accounts for 15% of the total decadal variance. The pattern of this REOF is similar to REOF3 of Mestas-Nunez and Enfield (1999) and REOF2 of Barlow et al. (2001), and has amplitudes predominantly in the eastern North Pacific, and is sometimes referred to as the Pacific decadal oscillation.
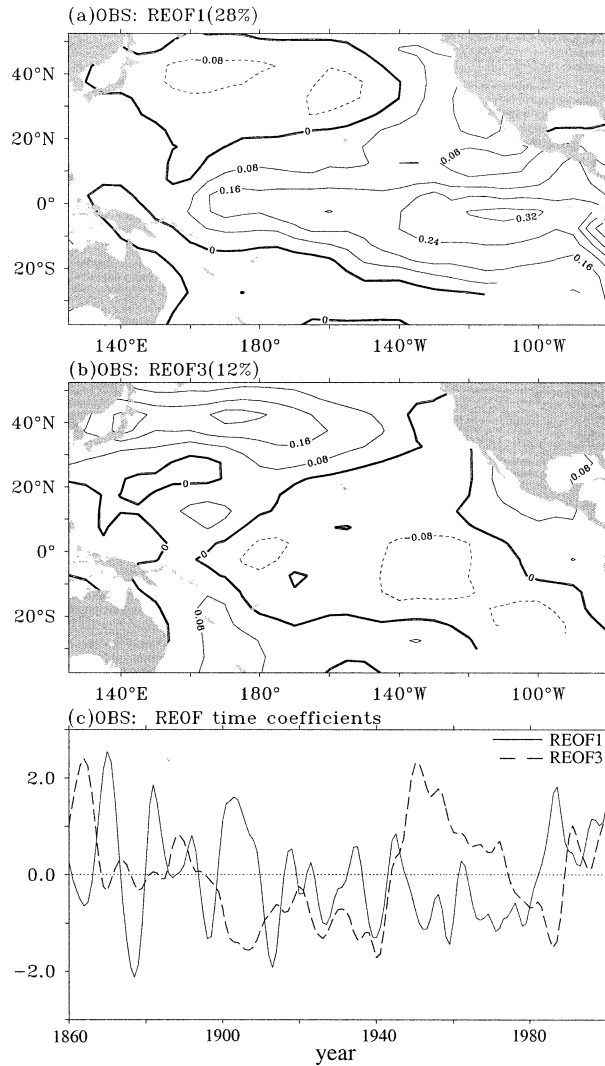
FIG. 1. Pacific basin REOFs of observed SSTAs: (a) REOF1, (b) REOF3, and (c) normalized time coefficient of REOF1 (solid) and REOF3 (dash). SSTAs are low-pass filtered to retain the variability longer than 8 yr. Contour interval is 0.08°C.
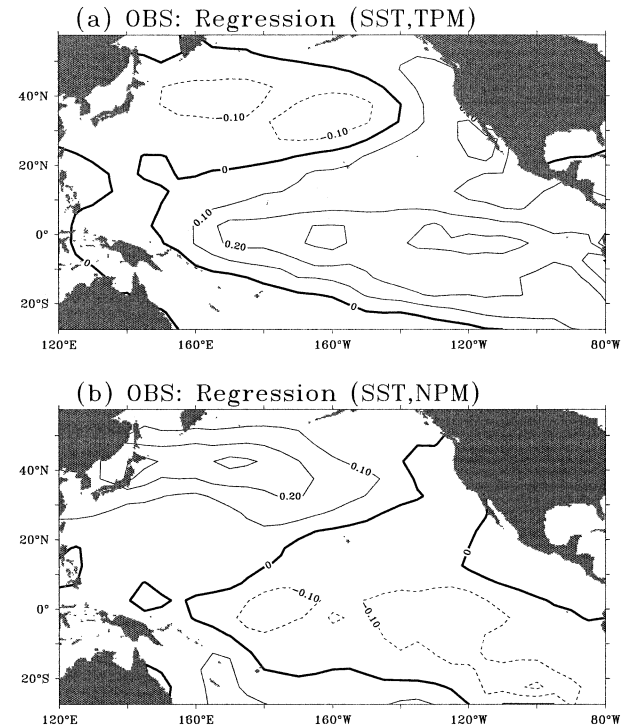

FIG. 2. Regression of Pacific basin low-pass-filtered SSTAs (observed) with SSTA time series (normalized) in the (a) tropical Pacific and (b) North Pacific. Contour interval is 0.1°C.

gime (1947–76), and back to a cold regime (from 1977 to at least the mid-1990s). The warm and cold episodes have a period of about 50–70 yr, which is consistent with previous studies (Mantua et al. 1997; Minobe 1997; D'Arrigo et al. 2001).

Further support for the existence of these two separate modes is obtained by regressing basin SST anomalies (SSTAs) against the SSTA averaged over the Niño-3 region (5°N–5°S, 120°–170°W) and the North Pacific (Figs. 2a,b), respectively. These two SST indices are correlated significantly with the time coefficients of the TPM (0.75) and NPM (0.88) indices, respectively. The autocorrelation function shows that the decorrelation timescale of SST is about 2–3 times longer in the North Pacific than the tropical Pacific (Fig. 3b). Furthermore, the correlation between these two SST indices is only about −0.36, implying little correspondence between them. SST regression patterns are broadly similar to the REOF patterns, with a spatial correlation of 0.92 and 0.95 for the TPM and NPM, respectively (Figs. 2a,b).

In summary, the analyses of observational SST data tentatively support the existence of a decadal–bidecadal tropical Pacific mode and a multidecadal North Pacific mode.

b. Model Pacific decadal variability

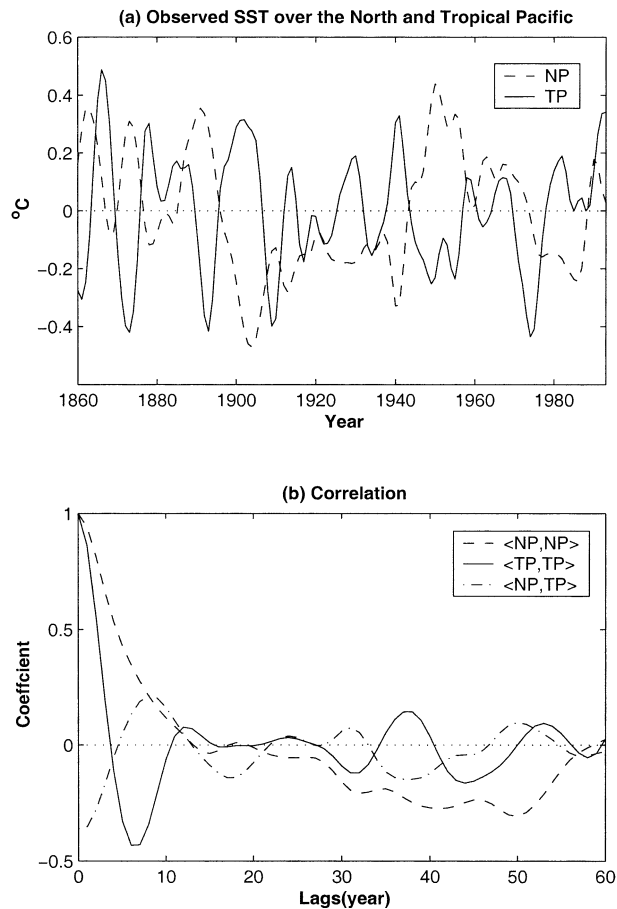We performed the same rotated EOF analysis on the SST simulated by the full coupled model (CTRL) as

mode is an ENSO-like mode (Fig. 1a), which for convenience here, will be referred to as the TPM because its loading is dominantly in the Tropics. The pattern is broadly similar to the "ENSO-like decadal" mode of Zhang et al. (1997), but with less signal in the North Pacific. The temporal evolution of this mode is characterized by decadal to bidecadal fluctuations (Fig. 1c). The third REOF shows variability predominantly in the North Pacific and will be referred to as the NPM. Modes with a similar structure have been found previously (Deser and Blackmon 1995; Nakamura et al. 1997; Mestas-Nunez and Enfield 1999; Barlow et al. 2001). In contrast to the TPM, the temporal evolution of the NPM seems to be characterized by a longer multidecadal timescale (Fig. 1c). The NPM as seen in Fig. 1c appears to evolve slowly from a cold regime (1890–1946) to a warm re-

(a) Observed SST over the North and Tropical Pacific

(b) Correlation

FIG. 3. (a) Low-pass-filtered SSTAs averaged over the North Pacific (30°–45°N, 140°E–170°W) (dash) and tropical Pacific (5°S–5°N, 180°–120°W) (solid) from the observation. (b) Autocorrelation of each time series and their cross correlation.

(a)CTRL REOF1 (21%)

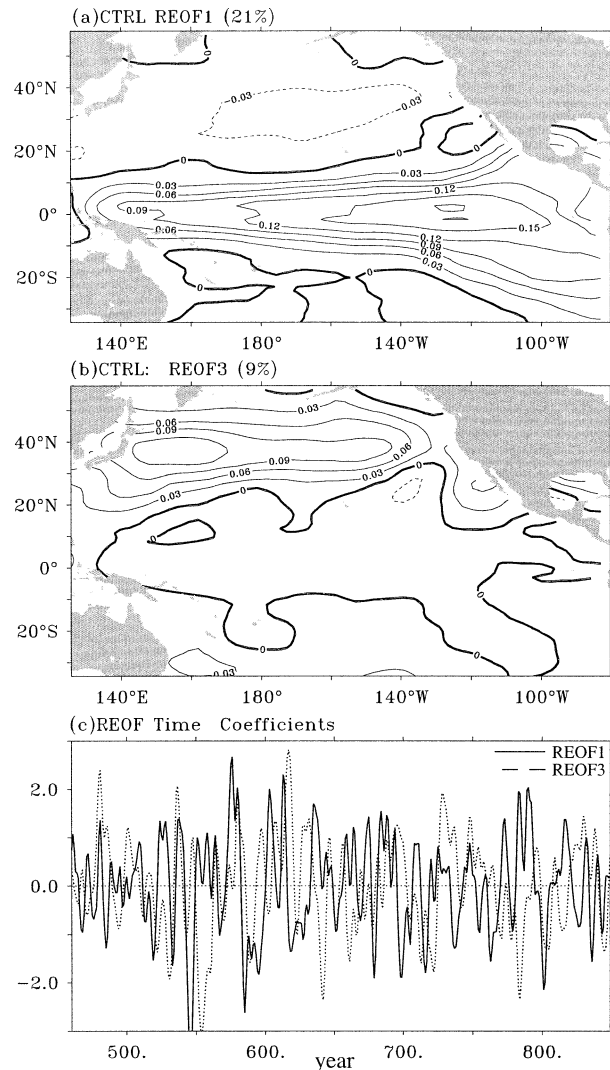(b)CTRL: REOF3 (9%)

(c)REOF Time Coefficients

FIG. 4. Pacific basin REOFs of 400-yr bandpass-filtered (8–200 yr) SSTAs in the CTRL run: (a) REOF1, (b) REOF3, and (c) normalized time coefficients of REOF1 (solid) and REOF3 (dash). Contour interval is 0.03°C.

was done for the observed SST. In addition to the 8-yr high-frequency cutoff, a 200-yr low-frequency cutoff was also applied in the analysis to remove any possible contribution from the effects of slow changes in the deep ocean.

The first and third REOF modes of the model SST (which explain 21% and 9% of the total decadal variance) correspond to the observed tropical and North Pacific modes, respectively (Fig. 4 versus Fig. 1). The pattern of the simulated TPM (Fig. 4a) is broadly similar to the observed (Fig. 1a) with a spatial correlation of 0.71. The simulated NPM also resembles the observed in the western to central North Pacific with a spatial correlation of 0.7, with both characterized by strong loadings along 40°N extending from Japan to 140°W.

As with the observations, additional support for the distinct TPM and NPM in the simulation is provided by regressing the basinwide SSTAs against the SST averaged in the tropical (7°S–7°N, 180°–120°W) and North (30°–45°N, 140°E–170°W) Pacific, respectively. The regression patterns virtually reproduce the two REOF modes (Fig. 5).

To examine whether these two modes have distinct oscillation timescales, the raw (unfiltered) data are projected onto the REOFs to obtain the projection time series, from which the power spectrum is computed (Saravanan and McWilliams 1997). The raw data, rather than filtered data, are used to ensure that any peaks in the spectrum are not simply an artifact of the time filter. The spectra of the time series associated with the TPM and NPM, obtained by multitaper spectrum analysis (Mann and Lees 1996), are shown in Fig. 6 along with the 50% and 95% confidence levels. We use three tapers in all the spectrum analyses in this study. Note that using more tapers will not change the conclusion drawn from the spectrum analyses, although the resolution of the spectrum is reduced. The spectrum of the TPM projection time series (Fig. 6a) shows significant variance at

(a)CTRL: Regression (SST,TPM)
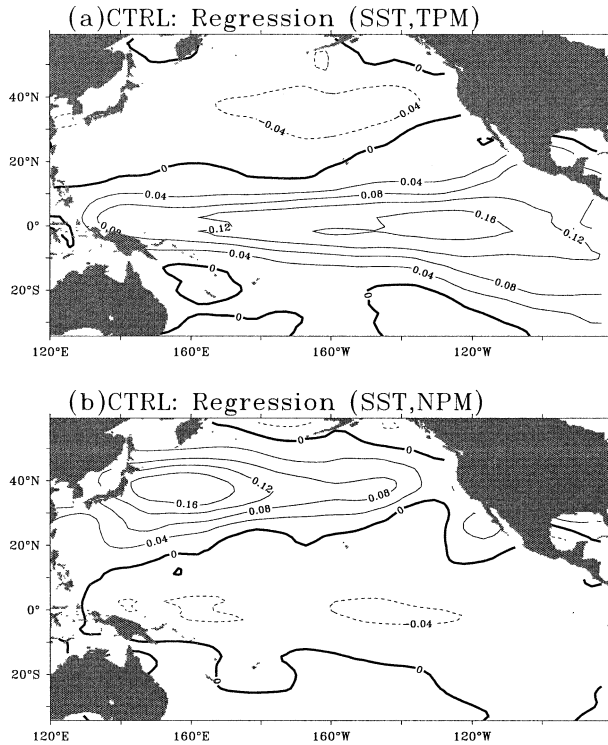

(b)CTRL: Regression (SST,NPM)

FIG. 5. Regression of Pacific basin low-pass-filtered SSTAs (CTRL) with SSTA averaged over (a) the tropical Pacific (7°S–7°N, 180°–120°W) and (b) North Pacific (30°–45°N, 140°E–170°W), respectively. Contour interval is 0.05°C.
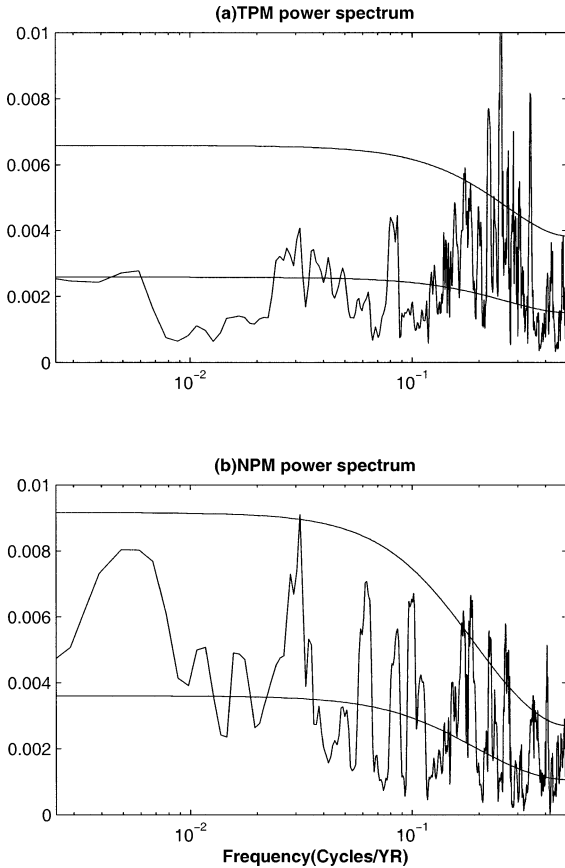
(a)TPM power spectrum

(b)NPM power spectrum

FIG. 6. Power spectrum of the projection times series (normalized) associated with the model-simulated (a) TPM and (b) NPM in CTRL. Levels of 50% and 95% statistical confidence are indicated.

interannual timescales with a dominant ENSO peak around 4 yr (Liu et al. 2000). The spectrum also shows some decadal to interdecadal variations notably around 14 and 30 yr. Relative to the tropical SST, the North Pacific SST is dominated by multidecadal variations (Fig. 6b). The spectrum of the projection time series associated with the TPM and NPM is similar to the spectra of the SSTA time series in the tropical and North Pacific, respectively (not shown).

Overall, the model appears to capture the major features of Pacific decadal variability in the observations, including the presence of two modes in the tropical and North Pacific, although the simulated modes are somewhat weaker than the observed by about 30% (Table 1).

While the above analysis provides some insight into Pacific decadal variability, it reveals little about the causes for these modes. This is because both the observed and fully coupled model climates are the product of complex interactions involving feedbacks that are not easily separated. In the following section, two surgical modeling strategies will be used to identify potential causes and mechanisms for these low-frequency variability modes.

4. Modeling surgery approach

a. Partial coupling (PC)

The first modeling surgery is the PC approach, which is used to help isolate the critical regions of ocean–

atmosphere coupling for generating decadal variability modes in the fully coupled model. In the PC experiments, the atmospheric model sees a prescribed annual cycle of SST that is obtained from the CTRL in a specified region (the PC region) and sees the predicted SST from the full ocean–atmosphere coupling elsewhere. The ocean model is forced by the full atmosphere–ocean

TABLE 1. Spatially averaged variances $[10^{-4}(°C)^2]$ of the decadal low-passed SSTs in the tropical (20°S–20°N) and North (20°–55°N) Pacific. The variance explained by the first EOF mode that is performed in the tropical and North Pacific domains is also given to represent part of coherent decadal variability in the tropical and North Pacific, respectively. All the experiments start from the same initial condition and are integrated for 400 yr.

	Decadal variance			
	Tropical Pacific		North Pacific	
	Total	EOF1	Total	EOF1
OBS	251	118	204	69
CTRL	180	80	177	50
PC-T	118	60	59	11
PC-ET	57	8	179	58
PBC-T	102	50	48	12
PC-G	45	5	57	12

flux calculated by the atmospheric model over the entire domain. Over the PC domain, the surface fluxes that drive the ocean model are calculated using SST predicted by the ocean model at each time step. Variability can still be generated in both the ocean and atmosphere in the PC region because of local atmospheric stochastic processes and interactions associated with remote sources of variability. Our one-way coupling over the PC domain has a stronger negative thermodynamic feedback, opposite to the other extreme case in which an ocean-alone experiment is forced by pure flux with no negative SST feedback at all. The former, relative to the fully coupled case, tends to overdamp the SST variability, while the latter overestimates SST variability (e.g., Saravanan and McWilliams 1997). The PC approach may underestimate atmospheric stochastic variability due to the fixed SST boundary condition (Barsugli and Battisti 1998). Nevertheless, the fixed SST forcing of the AGCM is a frequently used approach in AGCM experiments that can provide a useful reference to study the role of coupled ocean–atmosphere interaction in generating climate variability (e.g., Saravanan and McWilliams 1997; Chang et al. 2000).

b. Partial blocking (PB)

The second modeling surgery is the novel PB approach used as a means to assess the role of oceanic teleconnection. In the PB approach, ''sponge walls'' are placed at specified latitudinal bands of the ocean component of the coupled system such that the extratropical–tropical oceanic teleconnection is cut off. Within the sponge walls, temperature and salinity are restored toward the annual cycle of the CTRL run. Several PC/PB experiments are performed to identify the origins of the NPM and TPM; each is integrated for 400 yr without flux correction. The mean climatology of each experiment does not show any significant drift from the CTRL run.

5. The NPM and its origin

We now focus on two fundamental questions concerning the origins of decadal variability in the North Pacific. 1) Does the North Pacific decadal variability originate from local ocean–atmosphere interaction or remote tropical teleconnective forcing? 2) What is the role of coupled ocean–atmosphere feedbacks and atmospheric stochastic forcing in producing the decadal variability in the North Pacific?

The major conclusions from our PC and PB experiments are (i) the NPM is internal to the North Pacific region, supporting the conclusions drawn from the observations and the CTRL simulation; (ii) atmospheric stochastic forcing can produce a weak NPM-like mode in the North Pacific but with no preferred timescale, which is in contrast to Saravanan and McWilliams (1997) results; (iii) both ocean–atmosphere coupled

feedbacks and oceanic dynamics are needed to produce the multidecadal mode in the North Pacific.

a. The role of tropical teleconnective forcing

Previous studies have shown that ENSO can affect the North Pacific via atmospheric teleconnections (e.g., Horel and Wallace 1981; Graham 1994). However, observational evidence remains controversial as to whether the decadal variability in the North Pacific is directly driven by remote tropical teleconnective forcing (e.g., Deser and Blackmon 1995; Cane and Evans 2000). By comparing a fully coupled GCM experiment with a coupled AGCM–mixed layer ocean (to remove ENSO in the Tropics), some previous modeling studies have shown that North Pacific decadal variability is independent of the tropical teleconnective forcings (Barnett et al. 1999a). Such a modeling approach may shed light on the effect of tropical teleconnective forcing, but it may be inconclusive because the decadal mode in the North Pacific has been distorted due to a lack of ocean dynamics in the midlatitude mixed layer ocean, which has been shown to be critical for the generation of SST variability in the midlatitudes (e.g., Miller et al. 1998; Seager et al. 2001; Schneider et al. 2001; Pierce et al. 2001; Venzke et al. 2001).
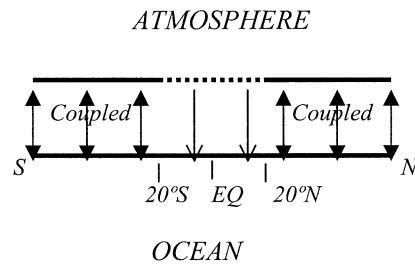
Here, we start our analyses with a PC experiment PC-ET (extratropics, Fig. 7a); in which tropical influence is removed by prescribing the climatological annual cycle of SST of the CTRL run equatorward of 20°. In the extratropics poleward of 20° (ET), full ocean–atmosphere coupling remains active as in the CTRL, and in contrast to a mixed layer ocean, full ocean dynamics in the extratropics remains the same as in the CTRL. By comparing CTRL with PC-ET, we can quantitatively assess the effect of tropical teleconnective forcing on the midlatitudes.

Without air–sea coupling in the Tropics (PC-ET), tropical SST variability is virtually removed (variance reduced by over 70% compared to CTRL; Table 1). The NPM appears as the first leading REOF mode in PC-ET (Fig. 8a), which explains 16% of the total decadal variance, compared to 9% in CTRL, and its pattern is broadly similar to that in CTRL (Fig. 4b) with a spatial correlation of 0.86. As for the NPM in CTRL, the central lobe of the mode is located along 40°N with the strongest loadings in the region of the Kuroshio Extension off Japan. The amplitude of the mode remains the same as that in CTRL. The message is as follows: the NPM is internal to the North Pacific climate system, generated predominantly by local ocean–atmosphere processes.
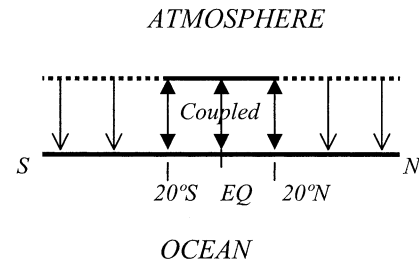
The spectrum of the projection time series associated with the leading REOF mode is shown in Fig. 9a1. While the spectrum of the NPM is essentially red in CTRL (Fig. 6b), the spectrum of the NPM in PC-ET shows a broad peak at around 40 to 50 yr (above the level of 95% statistical confidence). A similar power spectrum is found for the unfiltered SST averaged over
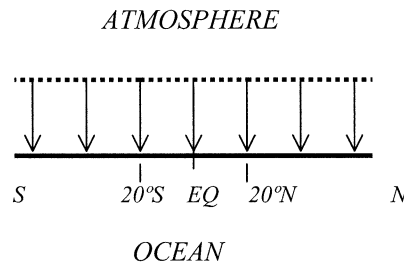
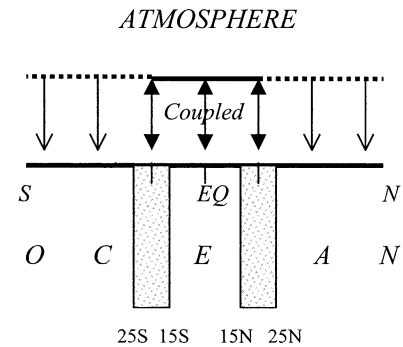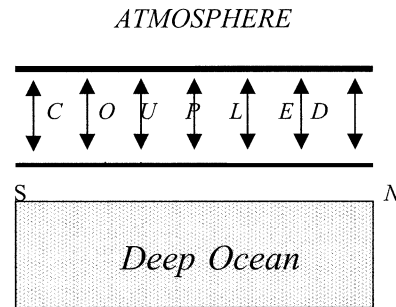**Partial Coupling and Partial Blocking Experiments**

(a) PC-ET

ATMOSPHERE

Coupled   Coupled

S   20°S EQ 20°N   N

OCEAN

(d) PC-T

ATMOSPHERE

Coupled

S   20°S EQ 20°N   N

OCEAN

(b) PC-G

ATMOSPHERE

S   20°S EQ 20°N   N

OCEAN

(e) PBC-T

ATMOSPHERE

Coupled

S   EQ   N

O   C   E   A   N

25S 15S   15N 25N

(c) PB-M

ATMOSPHERE

C O U P L E D

S   N

Deep Ocean

(f) PB_CTRL

ATMOSPHERE

C O U P L E D
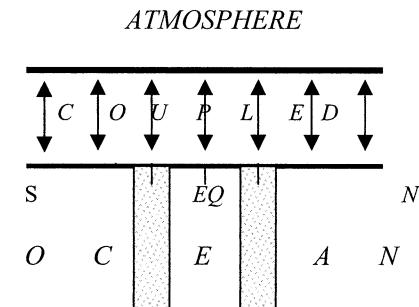
S   EQ   N

O   C   E   A   N

FIG. 7. Schematic diagram of PC and PB experiments. A dotted line represents the PC region where the model climatological SST is prescribed to force the atmosphere. A shaded block represents a PB sponge wall in which ocean temperature and salinity are restored toward the model's climatological annual cycle.

the domain of the maximum loading (30°–45°N, 140°E–140°W) (Fig. 9a2), confirming the robustness of the temporal behavior of the NPM.

The more pronounced multidecadal periodicy in PC-ET compared to the CTRL suggests that tropical teleconnective forcing may be able to distort the temporal behavior of the NPM even though it may not affect the magnitude. The specific process by which the tropical forcing affects the NPM remains to be studied in the future.

b. The role of local ocean–atmosphere coupling

We now examine whether the NPM arises from local ocean–atmosphere coupling or atmospheric stochastic forcing. Previous studies have shown differing results concerning the relative effects of local ocean–atmosphere coupling and stochastic forcing on the NPM. Some suggest that atmospheric forcing with spatial coherence can generate an oceanic variability mode with a preferred spatial and temporal scale (Saravanan and

(a) PC−ET: REOF1(16%)
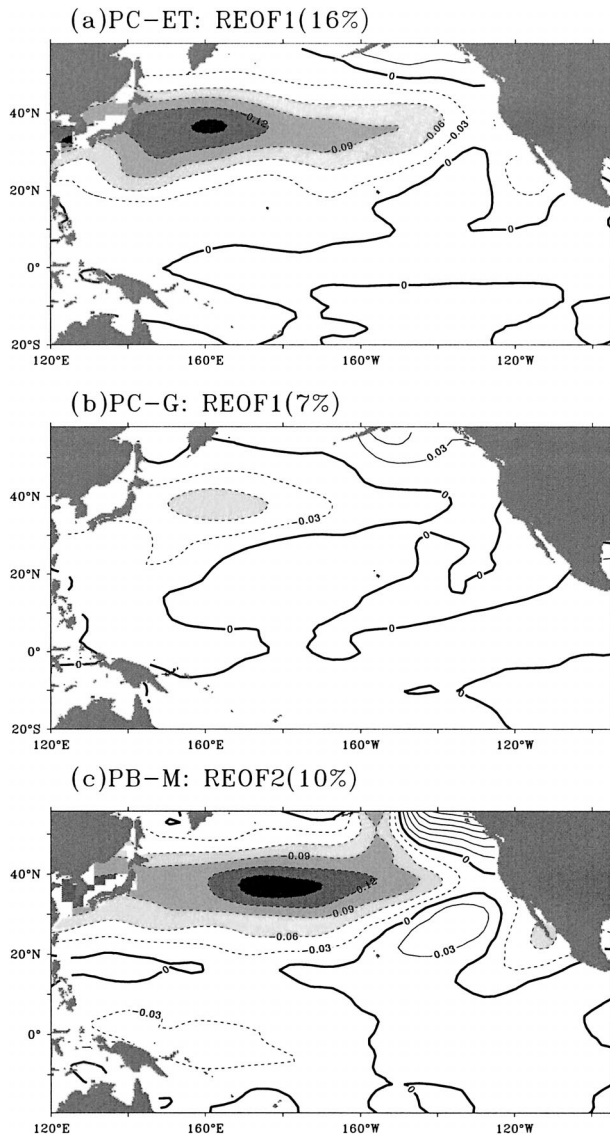
(b) PC−G: REOF1(7%)

(c) PB−M: REOF2(10%)

FIG. 8. The leading REOF modes of 400-yr bandpass (8–200 yr) filtered SSTAs in (a) PC-ET, (b) PC-G, and (c) PB-M experiments. Contour interval is 0.03°C. Areas with negative values exceeding 0.03°C are shaded.

McWilliams 1997; Jin 1997; Weng and Neelin 1998); others suggest that the dynamical feedback between the ocean and atmosphere in the North Pacific is crucial for the generation of the North Pacific mode (Latif and Barnett 1994, 1996). The NPM may also arise from atmospheric stochastic forcing, with ocean–atmosphere coupled feedbacks enhancing the variability and providing a regional interdecadal peak in the Kuroshio region off Japan (Barnett et al. 1999a). To address these controversial issues, we perform a PC experiment (PC-G), in which air–sea coupling is globally shut off by prescribing the model climatological SSTs over all the ocean basins (Fig. 7b).

Without air–sea coupling in the North Pacific, SST

decadal variability in the North Pacific is reduced by about 65% (compared with PC-ET; Table 1). Nevertheless, the leading REOF of SSTA in PC-G (which accounts for 7% of the variance) appears as an NPM-like mode (Fig. 8b). The mode captures some features of the NPM in CTRL and PC-ET with modest loadings in the Kuroshio Extension region, surrounded by some weak loadings of opposite sign along the west coast of North America. The dominant atmospheric variability modes in the North Pacific are also similar in PC-G, PC-ET, and the CTRL. Following Barnett et al. (1999a), we use the 500-mb geopotential height field in the domain (5°–60°N, 120°E–80°W) to represent the atmospheric low-frequency variability in the North Pacific. A standard EOF analysis is applied to the unfiltered annual data (The major conclusions are independent of the data filtering.) The leading EOF mode of the unfiltered data in the CTRL, PC-ET, and PC-G accounts for 30%, 31%, and 29% of the field variance, respectively (Fig. 10), with almost identical patterns (pattern correlations higher than 0.90). These patterns are similar to the patterns obtained in other higher-resolution models (Saravanan 1998; Barnett et al. 1999a).

In spite of the similar patterns of atmospheric and SST variability, the temporal behavior of the NPM differs significantly in these simulations. Without local ocean–atmosphere coupling in PC-G, the NPM has no preferred interdecadal timescale, as shown in the spectrum of the NPM projection time series (Fig. 9b1). The power spectrum of unfiltered SST anomalies averaged over the Kuroshio Extension is essentially red due to the ocean's memory (Fig. 9b2). This is in contrast to the coupled NPM mode in PC-ET, which shows a pronounced interdecadal timescale of 40 to 50 yr cycle^{-1} (Figs. 9a1, a2). The importance of coupled ocean–atmosphere feedback on the genesis of the NPM is also reflected in the atmospheric variability behavior. While the spectrum of the principal component of Z_{500} EOF1 is essentially white at decadal timescales in PC-G, PC-ET, and CTRL (Fig. 11), a significant peak of 30 to 40 yr cycle^{-1} is shown in the PC-ET Z_{500} EOF1 power spectrum (Fig. 11b), although the period is somewhat slightly shorter than that of the SST variations (versus Fig. 9a1). The role of ocean–atmosphere coupling can also be seen in the magnitude of atmospheric variability. Relative to PC-ET, while the total variance of Z_{500} height anomalies in PC-G is reduced modestly by 20%, the low-frequency variance (10–100 yr cycle^{-1}) is reduced substantially by 45%.

In summary, atmospheric stochastic forcing can give rise to an NPM-like low-frequency mode, but with no preferred timescale. In contrast, local ocean–atmosphere coupling is critical to the generation of the basin-scale NPM. Ocean–atmosphere coupling can enhance the strength of the NPM SST by about a factor of 2. In general, our modeling results are consistent with previous modeling studies of Barnett et al. (1999a), except the NPM in the FOAM has a broader spatial scale and
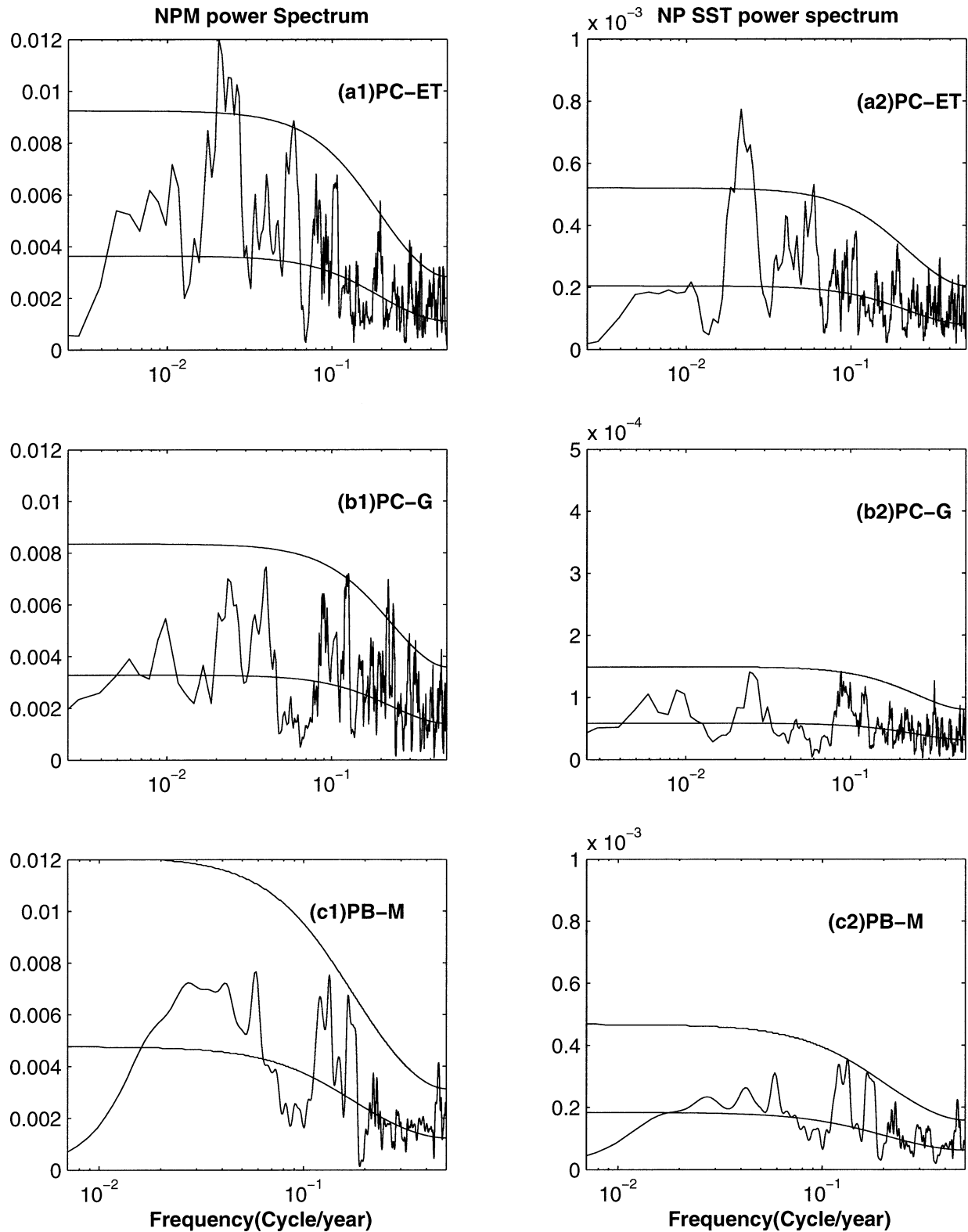
FIG. 9. (left) Power spectrum of the projection time series (normalized) associated with REOF1 in (a1) PC-ET, (b1) PC-G, and (c1) REOF2 in PB-M. (right) Power spectrum of unfiltered SST averaged over the loading center of REOF1 in (a2) PC-ET: (30°–45°N, 140°E–180°); (b2) PC-G: (30°–45°N, 140°E–180°); and (c2) PB-M: (30°–45°N, 160°E–160°W). Levels of 50% and 95% statistical confidence are indicated. Note that the PB-M experiment (mixed layer type) was run for 250 yr, while other experiments with full ocean dynamics were run for 400 yr.
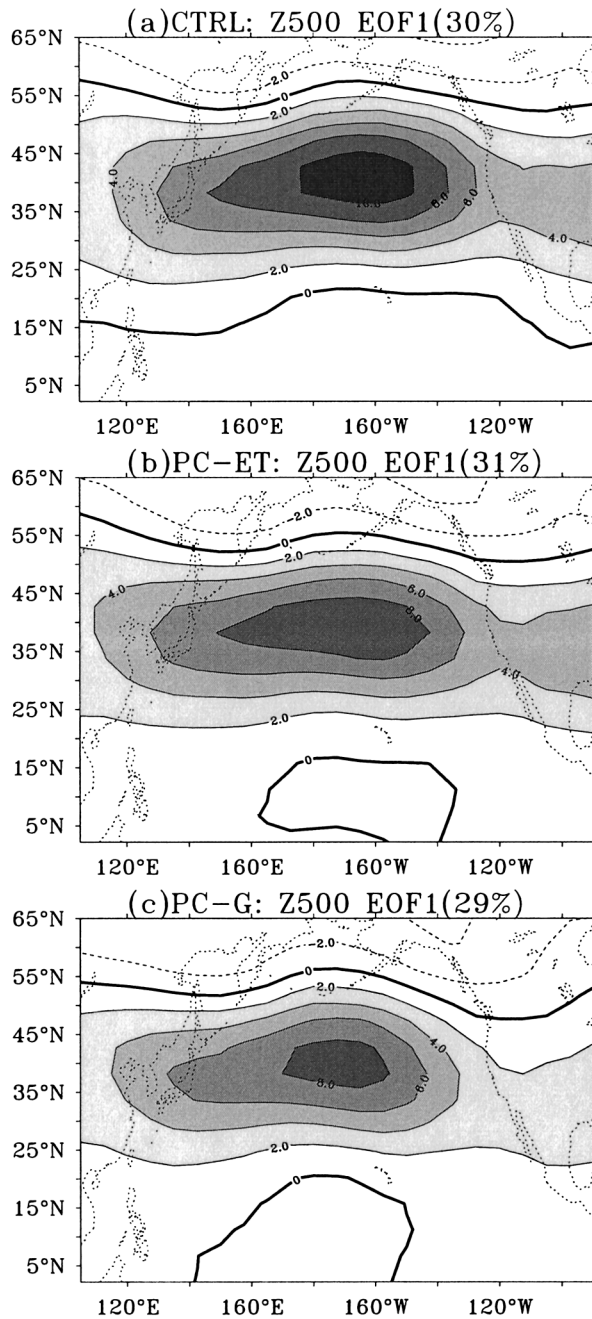
FIG. 10. EOF1 of annual 500-hPa height (Z_{500}) over the North Pacific: (a) CTRL, (b) PC-ET, and (c) PC-G. Contour interval is 2 m. Areas with value above 2 m are shaded.

FIG. 11. Power spectrum of the time coefficients (normalized) of EOF1 of the annual 500-hPa height (Z_{500}) over the North Pacific: (a) CTRL, (b) PC-ET, and (c) PC-G. Levels of 50% and 95% statistical significance are indicated.

a multidecadal period of 40–50 yr, rather than being geographically limited in the Kuroshio Extension off Japan with a shorter period of 20 yr.

c. The role of extratropical ocean dynamics

Previous studies proposed that decadal memory in the midlatitude ocean can be achieved by oceanic Rossby wave (e.g., Jin 1997; Weng and Neelin 1998) or gyre
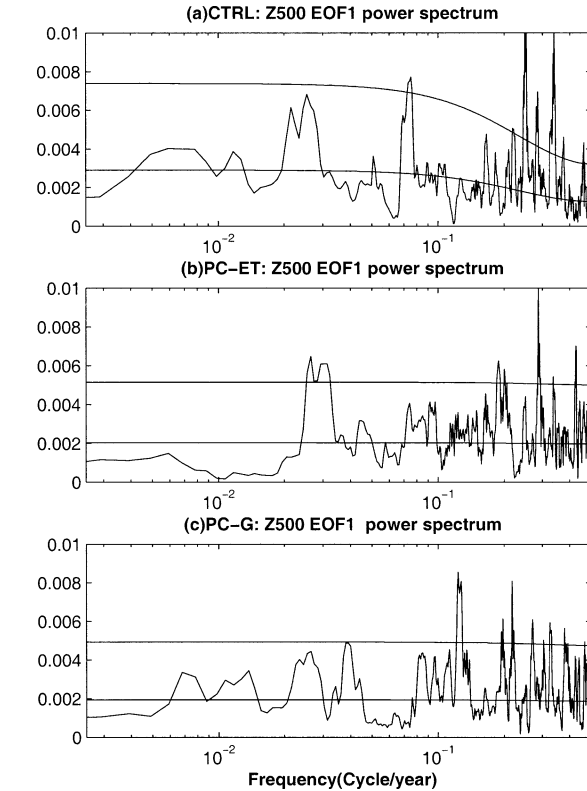
advection (e.g., Saravanan and McWilliams 1997; Latif and Barnett 1994, 1996). To assess the role of oceanic dynamics in generating the North Pacific mode, we start with an analysis of upper-ocean heat budget, and then investigate how ocean dynamics are involved in the life cycle of the NPM.

1) UPPER-OCEAN HEAT BUDGET

We regress the low-passed surface wind stress, turbulent heat flux (latent plus sensible heat flux) against SSTA in the Kuroshio Extension region for CTRL, PC-ET, and PC-G (Fig. 12). As a reference, the pattern of SST regression is also plotted. In all three experiments, warm (cold) SSTAs are accompanied by an anomalous anticyclonic (cyclonic) wind and anomalous easterlies (westerlies) in the midlatitudes. The heat flux tends to damp SSTAs over most of the Kuroshio Extension region, but enhances SSTAs immediately off and south of Japan. The damping effect of the heat flux on SSTAs in the Kuroshio Extension region appears to be consistent with previous studies (e.g., Frankignoul et al. 2000; Seager et al. 2001). This suggests that SSTAs in the Kuroshio Extension are likely produced by the change of ocean heat transport. We separate the change in ocean heat transport into the horizontal (advection) and ver-
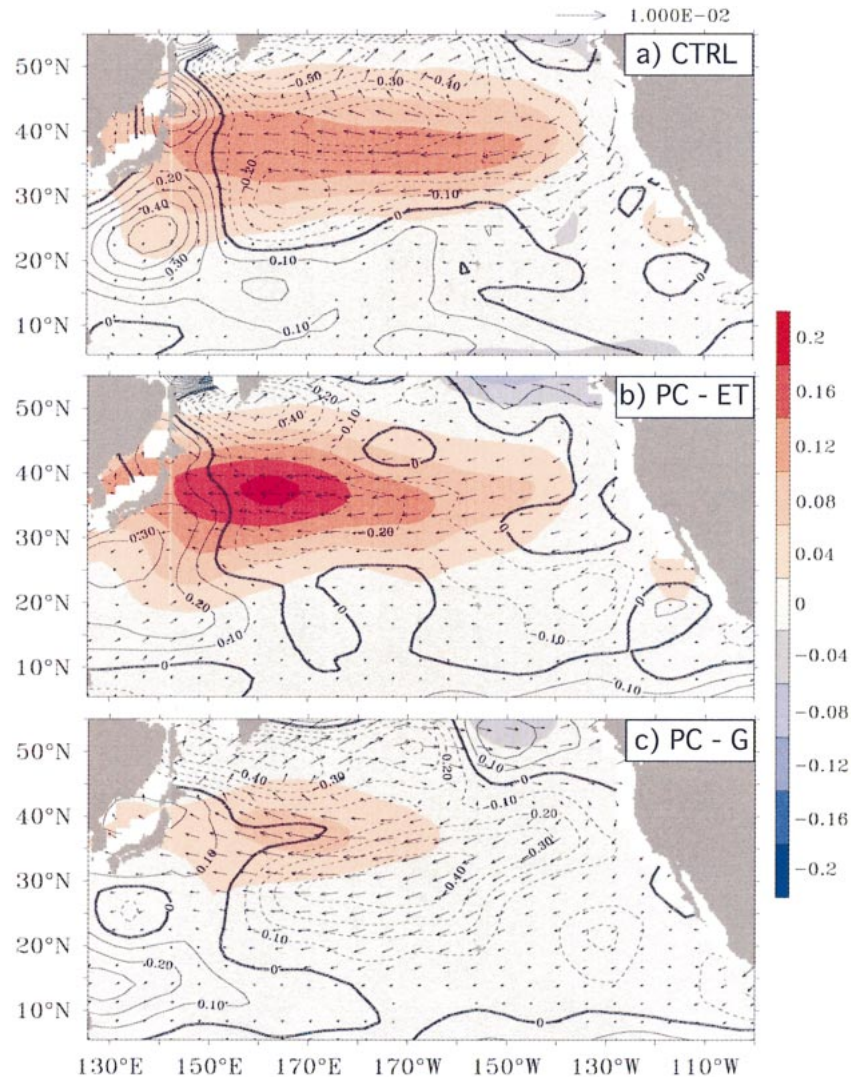
FIG. 12. Regression of wind stress, turbulent heat flux (latent plus sensible) with the normalized SST indices defined in Fig. 9. Regression of SSTAs are shaded as a reference. All data are bandpass filtered to retain variability between 8 and 200 yr: (a) CTRL, (b) PC-ET, and (c) PC-G. Contour interval for heat flux is 0.1 W m^{-2}. Downward heat flux is defined as positive in all panels. Unit of wind stress is N m^{-2}.

tical (advection, mixing, and convection) components, and regress them against the local SSTA, respectively. Figure 13 shows the zonal distribution of zero-lag regression coefficients of the upper 100-m heat budget terms (including net surface heat flux, oceanic zonal and meridional heat advection, and vertical heat transport) averaged in a latitudinal band around 40°N in PC-ET. Overall, warm (cold) SSTAs over the entire midlatitudes are predominantly associated with positive (negative) oceanic heat advection by the anomalous meridional ocean currents. A further analysis of the upper 50-m heat budget (not shown) shows that in the central Pacific (west of 170°E), SSTAs are associated predominantly with the advection of mean SST by the anomalous sur-

face Ekman drift, while in the Kuroshio Extension off Japan they are associated with advection by both surface and subsurface anomalous western boundary currents. In the region near Japan (west of 160°E), the surface heat flux combines with the meridional oceanic heat advection to enhance the SSTAs, whereas the vertical oceanic processes, predominantly convection processes, provide a strong damping to the SSTAs. An additional damping comes from the advection of SSTAs by the zonal mean current, which tends to move the SSTAs toward the east, and thus reduce SST variability in the region off Japan (west of 165°E), but enhance SST variability downstream (east of 165°E). In the central and eastern North Pacific (east of 170°W), the dominant
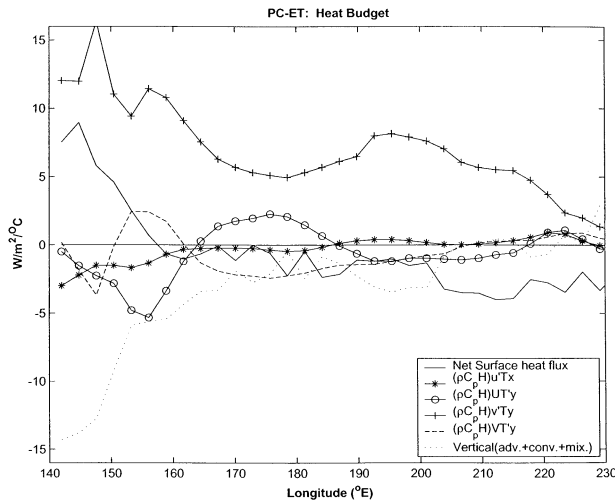
FIG. 13. Zonal distribution of zero-lag regression coefficients of terms in oceanic heat budget along 40°N in the experiment PC-ET. Each oceanic heat component is integrated over the upper 100 m, and then averaged over the latitudinal band of 35°–45°N after a band-pass filtering to retain variability between 8 and 200 yr, and finally regressed against the corresponding local SSTA along 40°N. Unit for each term is W m^{-2} K^{-1}. Primes represent anomalies.

positive meridional heat advection is balanced mainly by negative surface heat flux and oceanic vertical heat transport.

To further show the relative importance of surface Ekman flow and subsurface oceanic advection, we perform a mixed layer–type PB experiment, denoted PB-M (Fig. 7c). The configuration of the PB-M experiment is the same as the CTRL run except the temperature and salinity below 50 m are restored toward the climatology annual cycle of the CTRL run. The PB-M run is somewhat similar to a run with an atmospheric GCM coupled to a uniform 50-m-deep slab ocean mixed layer model, but with the surface Ekman flow included.

The second REOF mode in PB-M shows a NPM-like pattern, accounting for 10% of the field variance (Fig. 8c). Although the pattern is broadly similar to the NPM in PC-ET, differences due to the lack of subsurface oceanic dynamics are notable. Without subsurface oceanic dynamics, SST variability in the region off Japan is reduced, and the center of maximum variance shifts to the central Pacific around the date line (Fig. 8c versus 8a). Furthermore, in PB-M no significant interdecadal peaks occur in the power spectrum of the NPM mode projection time series. This is in contrast to PC-ET where subsurface oceanic dynamics is active (Fig. 9c1 versus 9a1); SST variance shows a substantial reduction at interdecadal timescales (Fig. 9c2 versus 9a2). In PB-M, SSTAs must be created by surface heat flux and/or heat advection by Ekman drift. In the central Pacific, SST variability remains significant and even stronger (Fig. 8c versus 8a), confirming the dominant effect of meridional oceanic heat advection by the surface Ekman flow, while in the region off Japan, SST variability

shows some modest reduction due to the absence of heat advection by the subsurface western boundary current. The effects of the surface heat flux in PB-M remains similar to that in PC-ET, which tends to enhance SSTAs in the region off Japan, but damp SSTAs in the Kuroshio Extension and Far East (not shown).

2) LIFE CYCLE OF THE NPM

How does subsurface ocean dynamics contribute to the interdecadal SST variations in the Kuroshio Extension off Japan? What oceanic processes account for the multidecadal timescale (40–50 yr) of the NPM? Several studies have suggested that SST anomalies in the Kuroshio Extension region are the delayed response to the change of the wind stress curl over the central Pacific (e.g., Seager et al. 2001; Schneider et al. 2002). To examine this delayed response in our model, we calculate the lagged regressions of SSTAs, upper 400-m ocean heat content, wind stress and curl, and surface heat flux (latent plus sensible) against SSTA in the region of the Kuroshio Extension in PC-ET (in which the cycle of the NPM is more prominent than the CTRL; Fig. 14). To show the life cycle of the NPM more clearly, all data are bandpass filtered to retain variability between 20 and 100 yr. The 0-lag regression corresponds to the mature warming phase, characterized by anomalous easterlies and the damping effect of surface heat flux in the region of the Kuroshio Extension (Fig. 14a1), positive heat content anomalies (HTAs), and antisymmetric wind curl over the extratropics (Fig. 14a2). The negative/positive wind curl anomalies in the subpolar/subtropical region simply reflect a northward shift of the subtropical–subpolar gyre boundary or an intensification of the Kuroshio Current. After that, the warm SSTAs slowly decay due to the damping of the surface heat flux (Figs. 14a1–c1), and the positive HTAs tend to propagate southwestward, seemingly following the subtropical gyre (Figs. 14a2–c2). At lag +8 yr, while the warm SSTA in the region of the Kuroshio Extension virtually disappears, a cold anomaly is initiated in the central Pacific as a response to local anomalous westerly wind whose origin has not been clearly identified (Fig. 14c1). As shown in the previous analysis of ocean heat budget, the cold SSTA in the central Pacific is created by the anomalous southward surface Ekman drift, which brings subpolar water to this region and makes the surface sufficiently cold so that the surface heat flux tends to damp the SSTA. Accompanying the cold SSTA is a negative HTA generated in the central Pacific in association with the positive wind curl anomalies (Fig. 14c2). After about 4 yr, a cold SSTA develops and the thermocline shallows in the region off Japan, while in the central Pacific, SSTA and HTA both grow and propagate slowly toward the west (Figs. 14d1–d2). Since the cold SSTA off Japan is predominantly created by the meridional ocean heat advection (shown by the analysis of the heat budget), the delayed response of the SSTA
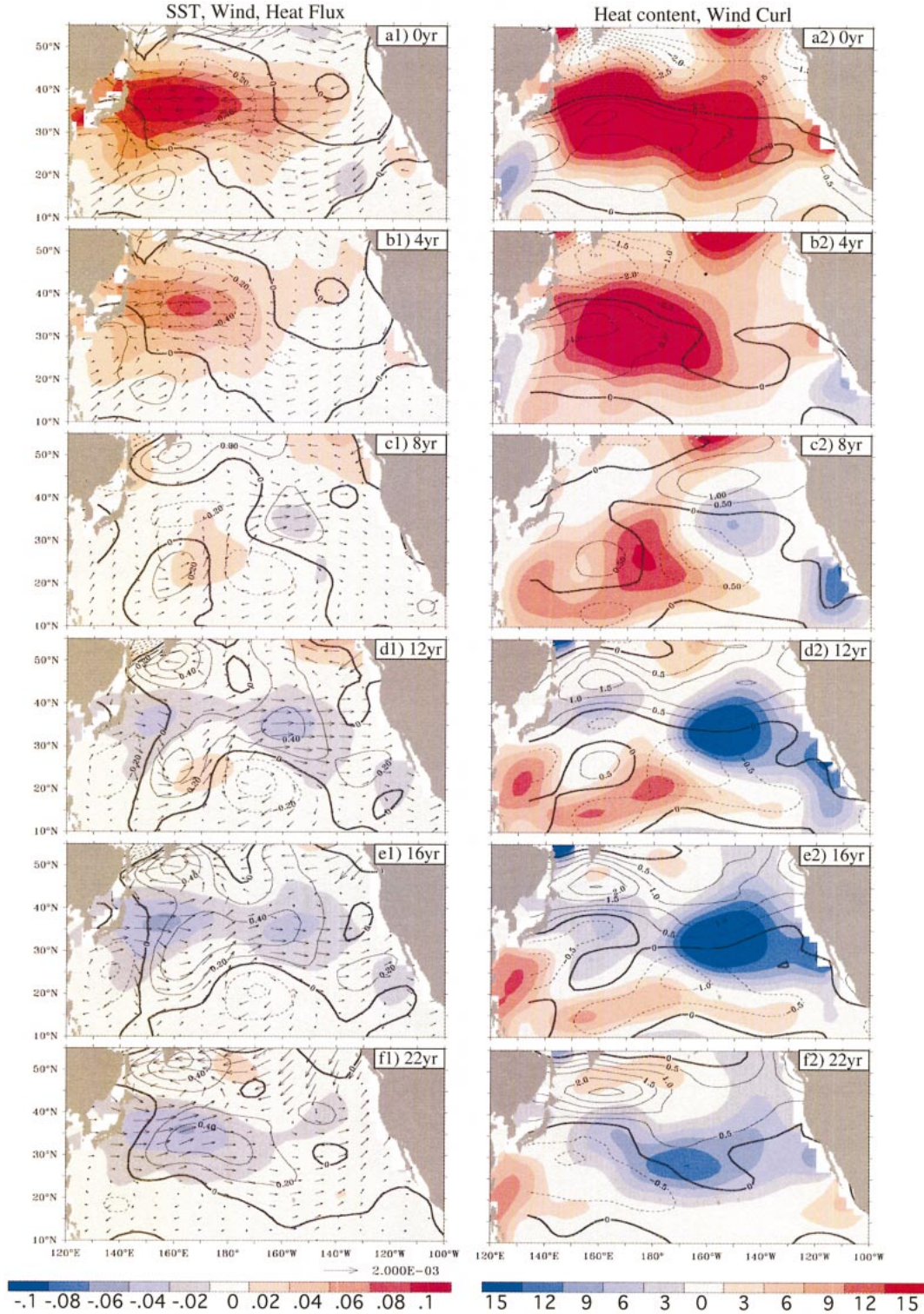
FIG. 14. Lagged regression of (a1)–(f1) wind stress and turbulent heat flux, (a2)–(f2) wind stress curl and ocean heat content with the normalized SST index defined in Fig. 9 for the experiment PC-ET. All data are bandpass filtered to retain variability between 20 and 100 yr cycle^{-1}. Lags are (a1), (a2) 0; (b1), (b2) 4; (c1), (c2) 8; (d1), (d2) 12; (e1), (e2) 16; (f1), (f2) 22 yr respectively. Contour intervals for heat flux and wind stress curl are 0.20 W m^{-2} and 3×10^{-10} N m^{-3}, respectively.

in this region can be understood in terms of gyre adjustment to the wind variations in the central Pacific. A positive wind curl in the central and eastern Pacific drives an anomalous northward interior Sverdrup flow, an equatorward shift of the subtropical–subpolar gyre boundary (after the passing of the planetary wave), a compensating southward western boundary flow from the subpolar gyre, and finally a cooling in the Kuroshio Extension off Japan. The cold SSTA off Japan is also enhanced by the surface heat flux, and subsequently propagates slowly toward the east where the surface heat flux acts to damp it (Figs. 14d1–f1). A similar eastward propagation is also shown by the HTAs in the region of the Kuroshio Extension (Figs. 14d2–f2). The slow growing/decay and eastward propagation of SSTAs, together with the delayed response of the western boundary current to the central North Pacific wind stress curl variation, may explain the multidecadal timescale of the North Pacific mode in our simulation.

In the model, there is an indication of negative feedback from the subtropical ocean as a response to the wind stress variation as previously suggested by Latif and Barnett (1994). For example, accompanying the positive curl of the wind stress in the subpolar region, a negative wind stress curl is generated in the subtropical region (Fig. 14c2), which enhances the positive HTAs that compensate the negative HTAs off Japan (Figs. 14d2–f2). However, such a negative feedback is overwhelmed by the effect of the shift of the subtropical–subpolar gyre boundary in the central and eastern North Pacific (Figs. 14c1–c2). In our model, causes for the initiation of the anomalous wind in the central North Pacific remain unclear. Conceivably, this response is related to the atmospheric response to midlatitude SSTA—a subject of considerable current debate (e.g., Kushnir et al. 2002), but one that is beyond of the scope of this study.

6. The TPM and its origins

Several hypotheses have been proposed for the origins of tropical Pacific decadal variability. Debates center around whether the tropical Pacific decadal variability is generated intrinsically in the tropical ocean–atmosphere system or involves remote North Pacific decadal variability via atmospheric and oceanic teleconnections. To assess the relative importance of local ocean–atmosphere interaction or extratropical–tropical atmospheric and oceanic teleconnection, we performed several PC/PB experiments. The major conclusions are 1) tropical Pacific variability originates predominantly from local ocean–atmosphere interactions; 2) extratropical–tropical teleconnections can enhance the TPM substantially, but are not necessary preconditions for the genesis of the TPM; and 3) the decadal memory in the Tropics seems to be associated with the high baroclinic modes of tropical oceanic waves.

a. The role of tropical ocean–atmosphere coupling

A partial coupling experiment (denoted PC-T, Fig. 7d) is performed in which the climatological annual cycle of SST from the CTRL run is prescribed poleward of 20° in both hemispheres, but full ocean–atmosphere coupling is allowed only in the Tropics (T). The PC-T experiment, together with the PC-ET experiment, allows us to assess the role of local ocean–atmosphere coupling versus remote forcing from the extratropics.

In PC-T, where ocean–atmosphere coupling is prevented in the extratropics, SST variability in the extratropics is reduced substantially by over 65% (Table 1). However, the TPM (REOF1 of SST) in PC-T, closely resembles the TPM in CTRL (spatial correlation 0.92) but with reduced variance (by about 25%—see Fig. 15b versus 15a and Table 1). The power spectrum of the TPM projection time series in PC-T shows a more pronounced peak at around 20–30 yr cycle^{-1} compared with the CTRL (Fig. 16a versus 6a). In contrast, without ocean–atmosphere coupling in the Tropics (PC-ET), none of the leading REOF SST modes resemble the TPM in CTRL and PC-T (not shown). The total decadal SST variance in the Tropics is reduced greatly by 70% relative to the CTRL (Table 1). These results indicate that *the TPM depends predominantly on local ocean–atmosphere coupling within the Tropics.*

The importance of local coupling in generating the TPM does not preclude remote impacts from the extratropics. The variance of the TPM, as already noted, is reduced by 25%, and the oscillation of the TPM tends to be more pronounced in PC-T than in CTRL. Nevertheless, the TPM may be influenced modestly by the remote variability from the extratropics via the atmospheric bridge, a result found in previous studies (e.g., Barnett 1999b; Vimont et al. 2001).

b. The role of extratropical–tropical oceanic teleconnection

The PC experiments above do not address the role of the extratropical–tropical oceanic bridge (e.g., Gu and Philander 1997) in the Tropics. This is because the subsurface oceanic temperature anomalies can still propagate between the Tropics and the extratropics. Indeed, based on PC-T alone, the TPM seems to be strongly associated with the slow adjustment of Rossby waves in the extratropics. Figure 17 shows the lagged regression of upper 200-m ocean HTA against the coefficient of REOF1 in PC-T. At the mature phase of an El Niño–like state (Fig. 18a1, lag 0), the equatorial thermocline shallows in the west and deepens in the east, corresponding to anomalous westerlies over the equator. Positive HTA in the eastern equatorial Pacific propagates poleward along the eastern boundary, generating a downwelling Rossby wave (Figs. 17a1–b1), which propagates westward in the subtropics and is reinforced by a negative wind stress curl along the 20°–30°N lat-

(a)CTRL: REOF1(21%)

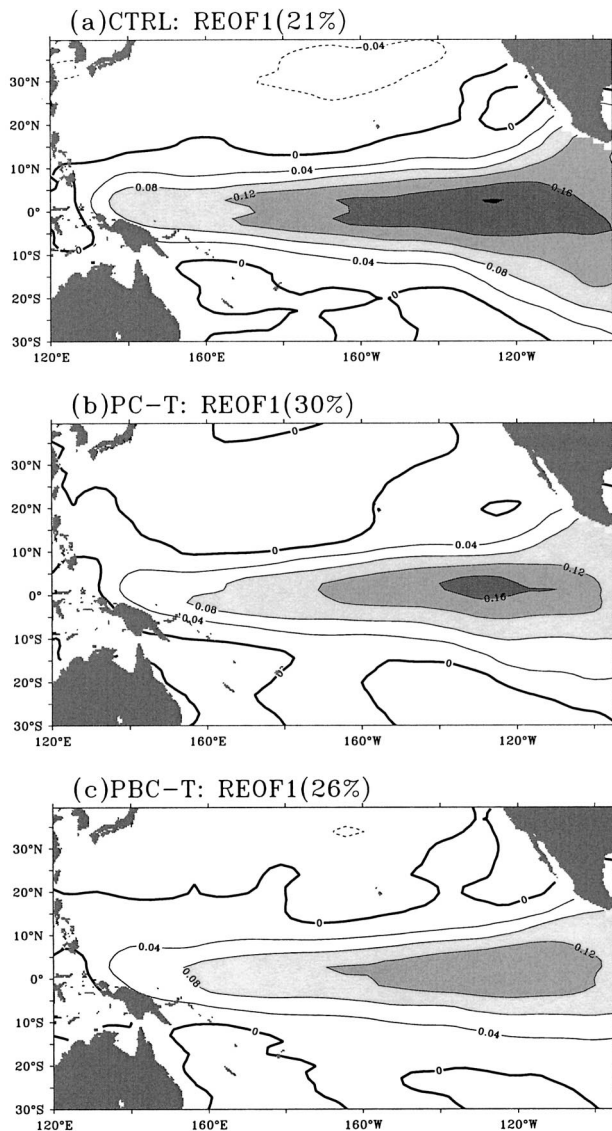

(b)PC-T: REOF1(30%)

(c)PBC-T: REOF1(26%)

FIG. 15. REOF1 in CTRL, PC-T, and PBC-T experiments. Areas with values above 0.08°C are shaded. Data are low-pass filtered (>8 yr) before performing EOFs.

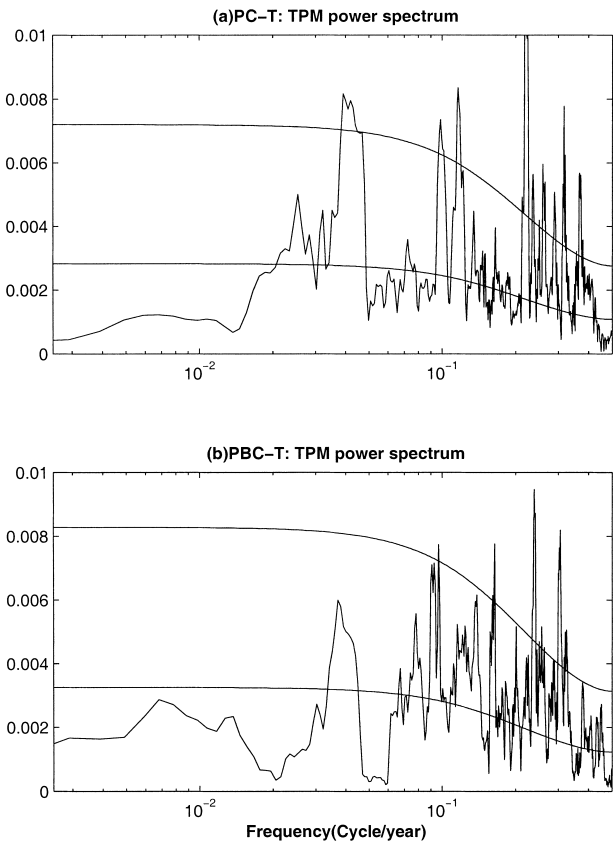(a)PC-T: TPM power spectrum

(b)PBC-T: TPM power spectrum

FIG. 16. Power spectrum of the TPM projection time series (normalized) in (a) PC-T and (b) PBC-T experiments. Levels of 50% and 95% confidence are indicated.

itudinal band (Figs. 17b1–c1). The negative wind stress curl is generated remotely by warm tropical SST, which intensifies the midlatitude westerlies via atmospheric teleconnection (Lau 1997). After about 9 yr, the positive HTA reaches the western boundary and penetrates into the western equatorial Pacific, reversing the negative HTA to a positive one (Figs. 17d1–e1). Note that in addition to the westward propagation, the extratropical HTA also seems to penetrate into the Tropics via an interior subduction pathway (Fig. 17d1). Similar features of wave propagation are also found in CTRL (not shown). This type of wave adjustment also seems to be present in other coupled models (e.g., Yukimoto et al 1996; Knutson and Manabe 1998).

To truly identify the role of extratropical–tropical oce-

anic teleconnection in the generation of the TPM, a partial blocking experiment is performed, in which extratropical–tropical oceanic teleconnections are shut off. The PB experiment shows that extratropical–tropical oceanic interaction, although it can intensify the TPM, is not a precondition for the genesis of the TPM.

The PB experiment, referred to as PBC-T (Fig. 7e), adopts the same configuration of ocean–atmosphere coupling as PC-T, but adds an oceanic sponge wall in the latitude band of 15°–25° in both hemispheres. The sponge wall extends from the surface to the bottom, within which a restoring term is added such that the temperature and salinity are restored toward the model's annual cycle climatology with a restoring time of 30 days.

In PC-T and PBC-T, both the timescale and intensity of ENSO remains virtually unchanged (not shown). This is expected because ENSO depends predominantly on topical ocean dynamics that are not altered significantly in the PB experiment.

Results show that the TPM is not changed significantly by cutting off extratropical–tropical oceanic teleconnection. Figure 15c shows that the REOF1 of the low-pass SST in PBC-T is virtually similar to that in PC-T, although its amplitude is reduced by about 15%–
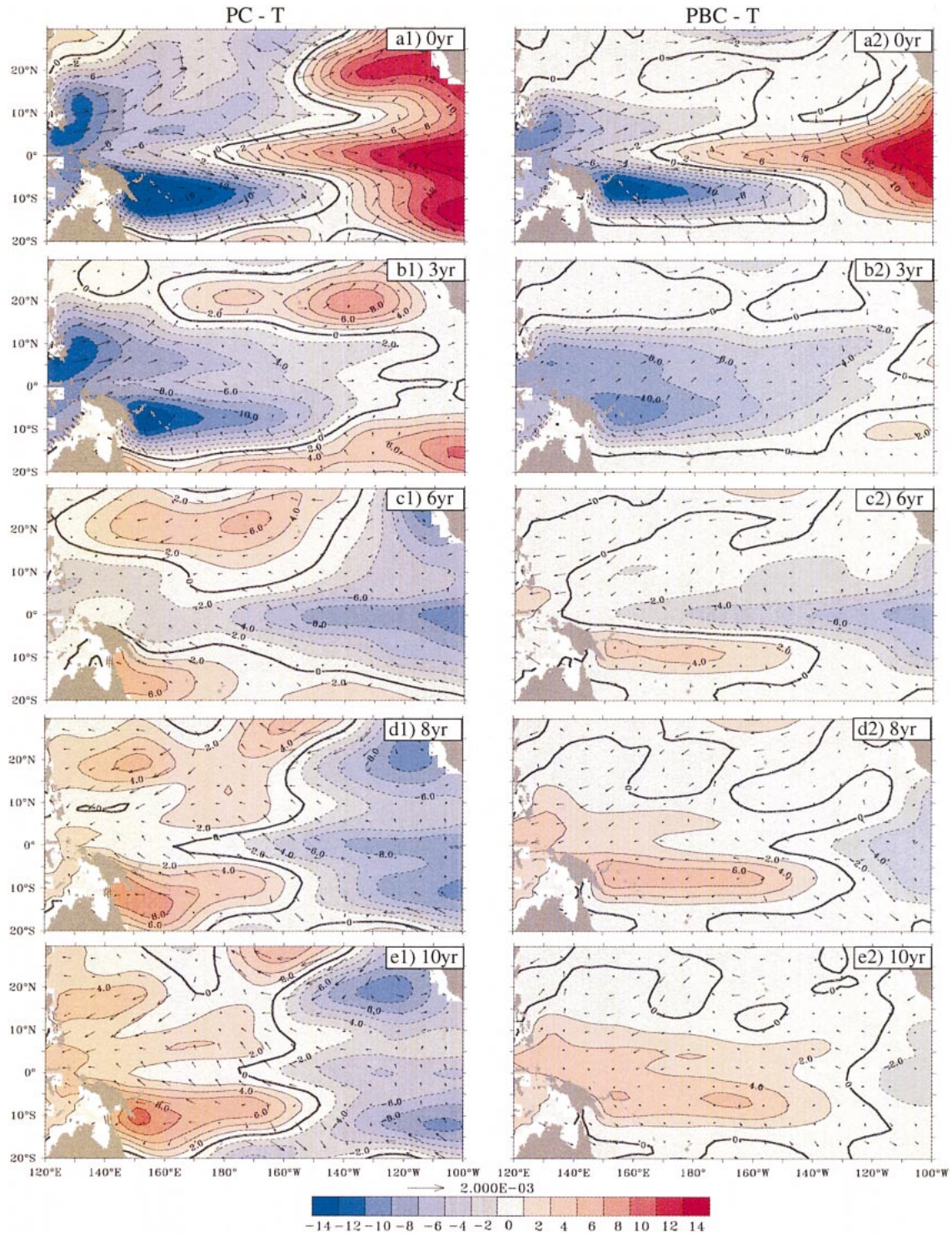
FIG. 17. Lagged regression of wind stress and ocean upper 200-m heat content with the temporal coefficient (normalized) of REOF1 in (a1)–(e1) PC-T and (a2)–(e2) PBC-T. All data including the regression index are bandpass filtered to retain variability between 10 and 40 yr cycle^{-1}. Units for heat content and wind stress are m °C^{-1} and N m^{-2}, respectively.
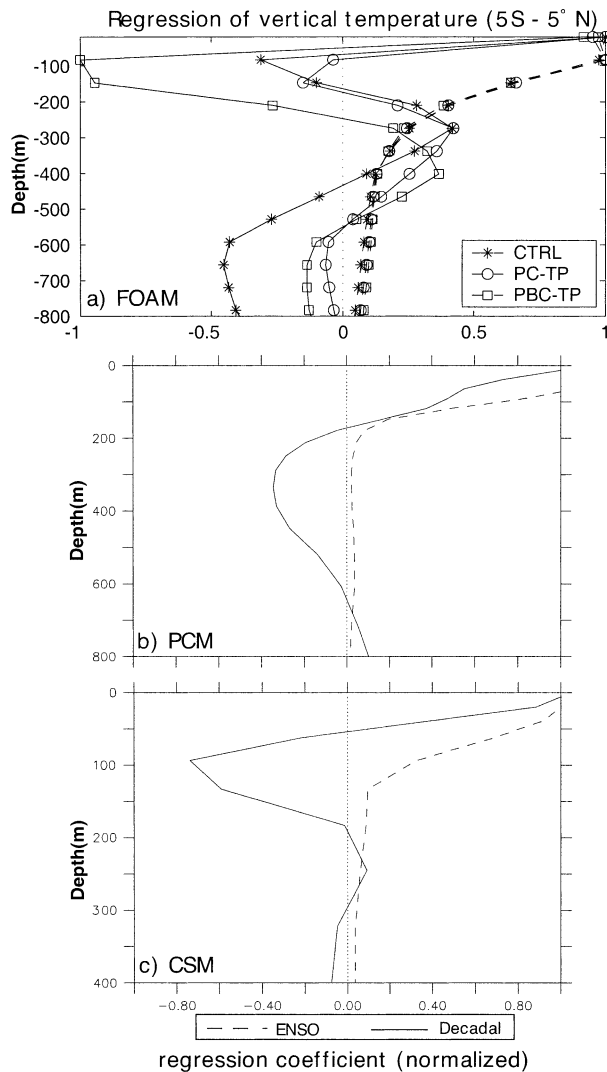
FIG. 18. Zonally averaged regression coefficients of equatorial vertical temperature (averaged in 5°S–5°N; normalized by the value on the surface). For decadal variability (solid), the low-passed temperature is regressed with the coefficient of EOF1 of SST in the tropical Pacific; for ENSO variability (dash), the residual high-passed temperature is regressed with the coefficient of the EOF1 of the high-passed SST: (a) FOAM (CTRL: stars; PC-T: open circles, PBC-T: squares); (b) PCM; and (c) CSM.

20% (Fig. 15c versus 15b and Table 1). The equatorial thermocline variability also remains similar in PBC-T and PC-T, except for the absence of heat content anomalies within the blocking zone (15°–25°) and along the eastern boundary in the off-equatorial region in PBC-T (Figs. 17a2–d2). The power spectrum of the TPM also shows a peak at about 20–30 yr cycle^{-1} although the statistical confidence is reduced from that in PC-T (Fig. 16b). The PBC-T run suggests that the origin of tropical Pacific decadal variability lies within 15° of the equator. In other words, most of the TPM is generated independently of the oceanic processes outside the Tropics. This is in contrast to the decisive role of extratrop-

ical–tropical oceanic teleconnection proposed by Gu and Philander (1997). In our experiments, oceanic teleconnection, although unnecessary for the generation of the TPM, can nevertheless modestly enhance the TPM.

The role of extratropical–tropical oceanic interaction on the TPM is also supported by an additional PB experiment, PB-CTRL (Fig. 7f), which allows full ocean–atmosphere coupling in both the extratropics and Tropics (as in CTRL), but has extratropical–tropical oceanic teleconnection cut off in the latitudinal band of 15°–25° as in PBC-T. Compared with CTRL, the pattern of the TPM in PB-CTRL remains largely unchanged (pattern correlation 0.95, not shown), while the variance is reduced by 18%. This result is consistent with the change from PC-T to PBC-T, further supporting the fact that extratropical–tropical oceanic interaction can enhance the TPM, but it is not a necessary condition for the TPM.

c. The role of tropical ocean dynamics: High baroclinic modes

In the absence of extratropical ocean memory, how is the decadal memory generated in the tropical Pacific in PBC-T? Previous studies suggest the possible role of nonlinearity (e.g., Münnich et al. 1991), ocean–atmosphere coupling (e.g., Neelin and Jin 1993), and the tropical basin mode (Jin 2001). With the tropical ocean basin now confined within 15° off the equator, the tropical ocean memory, taken as the slowest basin mode of a given baroclinic mode, is limited to the transient time of Rossby waves across the basin at 15° (Liu 2002). This transient time is at interannual timescales (for the first baroclinic mode) and cannot account for the decadal timescale of the TPM in PBC-T.

Alternatively, Liu et al. (2002) proposed that the tropical ocean may gain memory from higher baroclinic modes of tropical oceanic waves. Evidence of higher modes is seen in the spatial structure of the decadal temperature variability in the eastern tropical Pacific and are best illustrated in comparison with the interannual ENSO variability. The vertical structure of variability is illustrated by regressing the equatorial temperature averaged from 5°S to 5°N with the temporal coefficient of EOF1 of tropical Pacific SST (20°S, 20°N). We extend the analysis of Liu et al. (2002) to include two other simulations, one from a version of the NCAR Climate System Model (CSM; Otto-Bliesner and Brady 2001) and the other from the Parallel Climate Model (PCM; Meehl et al. 2001).

For ENSO, in all FOAM (CTRL, PC-T, and PBC-T) as well as CSM and PCM experiments, the temperature variability are meridionally trapped in the Tropics (<10°, not shown). In the vertical, the temperature variability is trapped near the surface and consists of a single polarity (<200 m, Figs. 18a–c). This suggests that ENSO is associated with the dynamics of the equa-

torial first baroclinic mode, as has been recognized in both observations and model studies. For decadal variability, the meridional structure extends to 30° in CTRL and PC-T, but only about 15° in PBC-T (not shown). In contrast to the meridional structure, for all experiments (FOAM, CSM, and PCM), the vertical regression of decadal temperature anomalies shows a consistent feature: the anomalies extend deeper, have a maximum confined in the thermocline, and change sign beneath the thermocline. This vertical phase structure of the decadal variability exhibits a higher baroclinic modal structure, in sharp contrast to the first modal structure of ENSO. This result suggests that tropical Pacific decadal variability is associated with higher baroclinic modes of tropical oceanic waves. The phase structures in Figs. 18a–c seem to suggest a third or fourth baroclinic mode for decadal variability that, according to the normal mode theory, should have a wave speed about 3–4 times slower than the first mode (Philander 1990). If one assumes a similar role of wave delay in decadal variability as for ENSO, the decadal variability should have a period of 3–4 times that of ENSO, or decadal to bidecadal timescales. However, this simple analogy to ENSO is very speculative at this stage. Further studies are in progress to better understand the nature of the higher baroclinic modes and their coupling with the atmosphere. Nevertheless, the robust vertical structure of the TPM in the five experiments and three independent models do suggest that high baroclinic modes of tropical oceanic waves could play important roles in the TPM.

7. Summary and discussion

The origin of Pacific decadal variability is investigated with a set of coupled ocean–atmosphere model experiments. Observations and model simulations suggest that Pacific decadal climate variability possesses two distinct modes: a decadal to bidecadal tropical Pacific mode (TPM) and a longer multidecadal North Pacific mode (NPM).

The simulated TPM originates predominantly from local ocean–atmosphere interaction within the Tropics. The long memory in the Tropics is associated with a higher mode of tropical baroclinic waves. In the meantime, the TPM is also enhanced substantially by extratropical–tropical interaction via atmospheric and oceanic teleconnections.

The simulated NPM originates from atmospheric stochastic processes and coupled ocean–atmosphere interaction locally within the extratropics. Atmospheric stochastic forcing can generate a weaker NPM-like pattern in both the atmosphere and ocean, but with no preferred timescales. Coupled ocean–atmosphere feedback and oceanic dynamics are needed to generate the basin-scale multidecadal mode in the North Pacific. The multidecadal memory seems to be associated with slow adjustment of subtropical/subpolar gyre in response to the wind stress variation and slow growing/decaying and
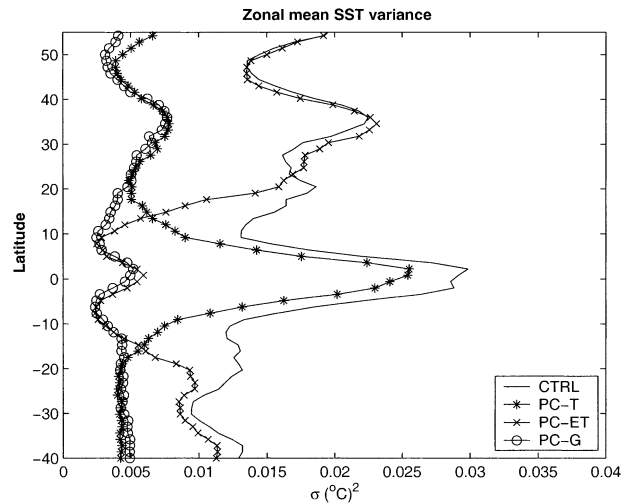

FIG. 19. Meridional distribution of zonal mean variance of bandpass (8–200 yr) filtered SST in CTRL (solid), PC-ET (cross), PC-T (star), and PC-G (circle).

eastward propagation of the SST anomalies in the region of the Kuroshio Extension. The advection of the mean temperature by the anomalous meridional ocean current plays a dominant role in creating these SST anomalies. In the central Pacific, cold (warm) SST anomalies are created by anomalous Ekman advection in response to the strengthening (weakening) of the midlatitude westerlies. In the Kuroshio Extension off Japan, SST anomalies are developed as a delayed response to the interior wind variation with a lag of about 5 yr, and enhanced by the surface heat flux. These SSTAs slowly propagate toward the east and are damped by the surface heat flux. The model indicates that the response of the atmosphere to SST in the Kuroshio Extension region may play a critical role in initiating the wind change in the interior that in turn causes SST changes, although the detailed response remains to be further studied.

The TPM and NPM also influence each other through teleconnections in the atmosphere and ocean. Indeed, each mode shows a more pronounced timescale of oscillation in the absence of the other (PC-T versus CTRL for the TPM; PC-ET versus CTRL for the NPM). This nonlinear interaction between the two modes is interesting and needs to be further studied in the future.

The relative importance of local coupling, atmospheric stochastic forcing, and extratropical–tropical teleconnective forcing in the generation of decadal variability of SST is summarized in the meridional distribution of the zonal mean of SST variance for PC-G, PC-ET, PC-T, and CTRL (Fig. 19). With the suppression of full ocean–atmosphere coupling, the SST variance in both the Tropics and extratropics is reduced substantially in PC-G by 85% and 60% in the tropical and North Pacific, respectively. The significant reduction of SST variability is due to the absence of local ocean–atmosphere coupling feedbacks and remote teleconnective forcing.

With the addition of full ocean–atmosphere coupling in the tropical Pacific alone, SST variance is enhanced from a stochastic level of 15% in PC-G to 80% in PC-T of the CTRL. The rest of the increase (the 20% difference between CTRL and PC-T) is predominantly contributed by the teleconnective forcing from the extratropics to the Tropics. With the addition of full ocean–atmosphere coupling in the North Pacific (but not the Tropics), total SST variance in the North Pacific is enhanced from the stochastic level of 30% in PC-G to over 90% in PC-ET (relative to the CTRL). The remaining slight increase (less than 10% difference between CTRL and PC-ET) is likely caused by the teleconnective forcing from the Tropics to the extratropics. Our PC experiments suggest that in the tropical Pacific, local ocean–atmosphere feedbacks dominate the effect of stochastic and teleconnective forcing, while in the North Pacific, ocean–atmosphere coupling and atmosphere stochastic processes are both important. The latter result here is somewhat consistent with the findings of Barnett et al. (1999a), who found that the coupled feedbacks substantially enhance atmospheric stochastically forced variability in the North Pacific.

Our modeling studies suggest that Pacific decadal variability is a complex phenomenon that may involve multiple origins and the interactions of the various modes. Further studies are clearly needed to examine some of the questions not fully answered in this paper. For example, for the North Pacific mode, it is still unclear how the atmosphere responds to SST anomalies in the midlatitudes to impact the NPM cycle. For the tropical Pacific mode, it remains unclear how the higher baroclinic modes of tropical oceanic waves couple to the atmosphere to generate slow coupled modes. Longer observational records are needed to verify the presence of the multidecadal modes, and longer simulations with other climate models are needed to test the robustness of the model results presented here.

Finally, we note that the modeling surgery strategies used here (partial coupling and partial blocking) provide potentially powerful tools for the understanding of the dynamics of climate variability in a coupled system. Here, we have demonstrated the utility of these tools in the understanding of multiple modes of decadal variability in the Pacific, supporting previous observational analyses.

REFERENCES

Barlow, M., S. Nigam, and E. H. Berbery, 2001: ENSO, Pacific decadal variability, and U.S. summertime precipitation, drought, and streamflow. *J. Climate,* **14,** 2105–2126.

Barnett, T. P., D. W. Pierce, R. Saravanan, N. Schneider, D. Dommenget, and M. Latif, 1999a: Origins of midlatitude Pacific decadal variability. *Geophys. Res. Lett.,* **26,** 1453–1456.

——, ——, M. Latif, D. Dommenget, and R. Saravanan, 1999b: Interdecadal interactions between the tropics and midlatitudes in the Pacific basin. *Geophys. Res. Lett.,* **26,** 615–618.

Barsugli, J. J., and D. S. Battisti, 1998: The basic effects of atmosphere–ocean thermal coupling on midlatitude variability. *J. Atmos. Sci.,* **55,** 477–493.

Cane, M., and M. Evans, 2000: Do the tropics rule? *Science,* **290,** 1107–1108.

Chang, P., R. Saravanan, L. Ji, and G. C. Hegerl, 2000: The effect of local sea surface temperatures on atmospheric circulation over the tropical Atlantic sector. *J. Climate,* **13,** 2195–2216.

D'Arrigo, R., R. Villalba, and G. Wiles, 2001: Tree-ring estimates of Pacific decadal climate variability. *Climate Dyn.,* **18,** 219–224.

Deser, C., and M. L. Blackmon, 1995: On the relationship between tropical and North Pacific sea surface temperature variations. *J. Climate,* **8,** 1677–1680.

Enfield, D. B., and A. M. Mestas-Nunez, 1999: Multiscale variability in global sea surface temperatures and their relationships with tropospheric climate pattern. *J. Climate,* **12,** 2719–2733.

Frankignoul, C., P. Muller, and E. Zorita, 1997: A simple model of the decadal response of the ocean to stochastic wind stress forcing. *J. Phys. Oceanogr.,* **27,** 1533–1546.

——, E. Kestenare, N. Sennechael, G. de Coetlogon, and F. D'Andrea, 2000: On decadal-scale ocean–atmosphere interactions in the extended ECHAM1/LSG climate simulation. *Climate Dyn.,* **16,** 333–354.

Garreaud, R., and D. Battisti, 1999: Interannual (ENSO) and interdecadal (ENSO-like) variability in the Southern Hemisphere tropospheric circulation. *J. Climate,* **12,** 2113–2123.

Graham, N. E., 1994: Decade-scale climate variability in the tropical and North Pacific during the 1970s and 1980s: Observations and model results. *Climate Dyn.,* **10,** 135–162.

Gu, D., and S. G. H. Philander, 1997: Interdecadal climate fluctuations that depend on exchange between the tropics and extratropics. *Science,* **275,** 805–807.

Hasselmann, K., 1976: Stochastic climate models. *Tellus,* **28,** 472–485.

Horel, J., and J. Wallace, 1981: Planetary-scale atmospheric phenomena associated with the Southern Oscillation. *Mon. Wea. Rev.,* **109,** 813–829.

Jacob, R. L., 1997: Low frequency variability in a simulated atmosphere–ocean system. Ph.D. thesis, University of Wisconsin—Madison, 155 pp.

Jin, F. F., 1997: A theory of interdecadal climate variability of the North Pacific Ocean–atmosphere system. *J. Climate,* **10,** 1821–1835.

——, 2001: Low-frequency modes of tropical ocean dynamics. *J. Climate,* **14,** 3874–3881.

Kaplan, A., M. A. Cane, Y. Kushnir, A. C. Clement, M. B. Blumenthal, and B. Rajagopalan, 1998: Analysis of global sea surface temperatures 1856–1991. *J. Geophys. Res.,* **103,** 18 567–18 589.

Kleeman, R., J. P. McCreary, and B. A. Klinger, 1999: A mechanism for generating ENSO decadal variability. *Geophys. Res. Lett.,* **26,** 1743–1746.

Knutson, T. R., and S. Manabe, 1998: Model assessment of decadal variability and trends in the tropical Pacific Ocean. *J. Climate,* **11,** 2273–2296.

Kushnir, Y., W. A. Robinson, I. Bladé, N. M. J. Hall, S. Peng, and R. Sutton, 2002: Atmospheric GCM response to extratropical SST anomalies: Synthesis and evaluation. *J. Climate,* **15,** 2233–2256.

Latif, M., and T. P. Barnett, 1994: Causes of decadal climate variability over the North Pacific and North America. *Science,* **266,** 634–637.

——, and ——, 1996: Decadal climate variability over the North Pacific and North America: Dynamics and predictability. *J. Climate,* **9,** 2407–2423.

Lau, N. C., 1997: Interactions between global SST anomalies and the midlatitude atmospheric circulation. *Bull. Amer. Meteor. Soc.,* **78,** 21–33.

Liu, Z., 2002: How long is the memory of tropical ocean dynamics? *J. Climate,* **15,** 3518–3522.

——, S. G. H. Philander, and R. Pacanowski, 1994: A GCM study of tropical–subtropical upper-ocean mass exchange. *J. Phys. Oceanogr.,* **24,** 2606–2623.

——, J. Kutzbach, and L. Wu, 2000: Modeling climatic shift of El Niño variability in the Holocene. *Geophys. Res. Lett.,* **27,** 2265–2268.

——, L. Wu, R. Gallimore, and G. Jacob, 2002: Search for the origins of Pacific decadal climate variability. *Geophys. Res. Lett.,* **29** (10), 1404, doi:10.1029/2001GL013735.

Lysne, J., P. Chang, and B. Giese, 1997: Impact of the extratropical Pacific on equatorial variability. *Geophys. Res. Lett.,* **24,** 2589–2592.

Mann, M., and J. Lees, 1996: Robust estimation of background noise and signal detection in climate time series. *Climatic Change,* **33,** 409–445.

Mantua, N. J., S. R. Hare, Y. Zhang, J. Wallace, and R. C. Francis, 1997: A Pacific interdecadal climate oscillation with impacts on salmon production. *Bull. Amer. Meteor. Soc.,* **78,** 1069–1079.

McCreary, J. P., and P. Lu, 1994: Interaction between the subtropical and equatorial ocean circulations: The subtropical cell. *J. Phys. Oceanogr.,* **24,** 466–497.

Meehl, G., J. Arblaster, B. Otto-Bliesner, E. Brady, and A. Craig, 2001: Factors that affect amplitude of El Niño in global coupled climate models. *Climate Dyn.,* **7,** 515–526.

Mestas-Nunez, A. M., and D. B. Enfield, 1999: Rotated global modes of non-ENSO sea surface temperature variability. *J. Climate,* **12,** 2734–2746.

Miller, A. J., and N. Schneider, 2000: Interdecadal climate regime dynamics in the North Pacific Ocean: Theories, observation and ecosystem impacts. *Progress in Oceanography,* Vol. 27, Pergamon, 257–260.

——, D. R. Cayan, and W. B. White, 1998: A westward intensified decadal change in the North Pacific thermocline and gyre-scale circulation. *J. Climate,* **11,** 3112–3127.

Minobe, S., 1997: A 50–70 year climate oscillation over the North Pacific and North America. *Geophys. Res. Lett.,* **24,** 683–686.

Münnich, M., M. A. Cane, and S. E. Zebiak, 1991: A study of self-excited oscillations in a tropical ocean–atmosphere system. Part II: Nonlinear cases. *J. Atmos. Sci.,* **48,** 1238–1248.

Nakamura, H., G. Lin, and T. Yamagata, 1997: Decadal climate variability in the North Pacific during recent decades. *Bull. Amer. Meteor. Soc.,* **78,** 2215–2225.

Neelin, J. D., and F. F. Jin, 1993: Modes of interannual topical ocean–atmosphere interaction—A unified view. Part II: Analytical results in the weak-coupling limit. *J. Atmos. Sci.,* **50,** 3504–3522.

Nitta, T., and S. Yamada, 1989: Recent warming of tropical sea surface temperature and its relationship to the Northern Hemisphere circulation. *J. Meteor. Soc. Japan,* **67,** 187–193.

Otto-Bliesner, B., and E. Brady, 2001: Tropical Pacific variability in the NCAR Climate System Model. *J. Climate,* **14,** 3587–3607.

Philander, S. G. H., 1990: *El Niño, La Niña, and the Southern Oscillation.* Academic Press, 293 pp.

Pierce, D. W., T. P. Barnett, and M. Latif, 2000: Connections between the Pacific Ocean Tropics and midlatitudes on decadal timescales. *J. Climate,* **13,** 1173–1194.

——, ——, N. Schneider, R. Saravanan, D. Dommenget, and M. Latif, 2001: The role of ocean dynamics in producing decadal climate variability in the North Pacific. *Climate Dyn.,* **18,** 51–70.

Saravanan, R., 1998: Atmospheric low-frequency variability and its relationship to midlatitude SST variability: Studies using the NCAR Climate System Model. *J. Climate,* **11,** 1386–1404.

——, and J. C. McWilliams, 1997: Stochasticity and spatial resonance in interdecadal climate fluctuations. *J. Climate,* **10,** 2299–2320.

Schneider, N. S., 2000: A decadal spiciness mode in the tropics. *Geophys. Res. Lett.,* **27,** 257–260.

——, A. J. Miller, and D. Pierce, 2002: Anatomy of North Pacific decadal variability. *J. Climate,* **15,** 586–605.

Seager, R., Y. Kushnir, N. Naik, M. Cane, and J. Miller, 2001: Wind-driven shifts in the latitude of the Kuroshio–Oyashio Extension and generation of SST anomalies on decadal timescales. *J. Climate,* **14,** 4249–4266.

Trenberth, K. E., 1990: Recent observed interdecadal climate change in the Northern Hemisphere. *Bull. Amer. Meteor. Soc.,* **71,** 988–993.

——, and J. W. Hurrell, 1994: Decadal atmosphere–ocean variations in the Pacific. *Climate Dyn.,* **9,** 303–319.

Tziperman, E., M. A. Cane, and S. E. Zebiak, 1995: Irregularity and locking to the seasonal cycle in an ENSO prediction model as explained by the quasi-periodicity route to chaos. *J. Atmos. Sci.,* **52,** 293–306.

Venzke, S., M. Muennich, and M. Latif, 2001: On the predictability of decadal changes in the North Pacific. *Climate Dyn.,* **16,** 379–392.

Vimont, D., D. Battisti, and A. Hirst, 2001: Footprinting: A seasonal connection between the midlatitudes and tropics. *Geophys. Res. Lett.,* **28,** 3923–3927.

Weng, W., and J. Neelin, 1998: On the role of ocean–atmosphere interaction in midlatitude interdecadal variability. *Geophys. Res. Lett.,* **25,** 167–170.

Wu, L., and Z. Liu, 2002: Is Tropical Atlantic Variability driven by the North Atlantic Oscillation? *Geophys. Res. Lett.,* **29** (13), 1653, doi:10.1029/2002GL014939.

Yukimoto, S., M. Eudoh, K. Kitamura, A. Kitoh, T. Motoi, A. Noda, and T. Tokioka, 1996: Interannual and interdecadal variabilities in the Pacific in an MRI coupled GCM. *Climate Dyn.,* **12,** 667–683.

Zhang, Y., J. M. Wallace, and D. S. Battisti, 1997: ENSO-like interdecadal variability: 1900–1993. *J. Climate,* **10,** 1004–1020.